Journal of Operation and Automation in Power Engineering
Vol. 11, No. 2, Aug. 2023, Pages: 83-93
http://joape.uma.ac.ir

A New Robust Load Frequency Controller for Electric Vehicle Aggregators

S. Malek, A. Khodabakhshian*, R. Hooshmand

Department of Electrical Engineering, University of Isfahan, Isfahan, Iran

Abstract- *This paper proposes a robust state feedback controller for Electric Vehicle aggregators to solve the challenging problem caused by the participation of Electric Vehicles in the load frequency control of the power system. The Lyapunov-Krasovskii functional method is used to achieve two objectives of the robust performance and stability. Then, by using teaching learning based optimization algorithm, both primary and secondary participation gains of EV aggregators in LFC are optimally determined. The Generation Rate Constraint and time delay, as nonlinear elements, are also taken into account. Simulations are carried out on two nonlinear power systems by using the power system simulation software. The results show that the designed controller gives a desirable robust performance for frequency regulation at the presence of uncertainties.*

Keyword: Electric Vehicle Aggregator, Frequency Control, Linear Matrix Inequality, Teaching Learning Based Optimization.

NOMENCLATURE

i	Subscript showing the number of area
R	Droop coefficient (pu)
D	Damping factor (pu)
M	Inertia (s)
T_{ij}	Tie-line synchronizing coefficient between the i-th and j-th power areas (pu)
K_I	Integral controller gain
β	Bias factor (pu)
ΔP_L	Load demand change (pu)
ΔP_v	Output power of governor deviation (pu)
ΔP_m	Output power of turbine deviation (pu)
ΔP_{EV}	Output power of EV aggregator deviation (pu)
$\Delta P_{\text{tie-line}}$	Tie-line power deviation (pu)
T_G	Governor time constant (s)
T_T	Turbine time constant (s)
T_{EV}	Time constant of EV model (s)
$K_{P,EV}$	Primary contribution setting of EVs
$K_{S,EV}$	Secondary contribution setting of EVs
$K_P^{\max}$	Maximum value for K_P
$K_S^{\max}$	Maximum value for K_S
K_{SF}	State feedback vector
Δu_C	Output deviation of the secondary controller for generators (pu)
Δu	Output deviation of the secondary controller of EVs (pu)
w	Disturbance originating from effect of the neighbor areas
z	Measurement variable
ACE	Area Control Error (pu)
τ_1	Time delay associated to secondary control of generators (s)
τ_2	Time delay associated to the secondary control of EV aggregators (s)

Received: 30 Oct. 2021
Revised: 07 Dec. 2021
Accepted: 23 Feb. 2022
*Corresponding author:
E-mail: aminkh@eng.ui.ac.ir (A. Khodabakhshian)
DOI: 10.22098/joape.2023.9749.1682
Research Paper

1. INTRODUCTION

Nowadays, Electric Vehicle (EV) integration into the power system is being increased and their ability in V1G (vehicle to grid integration) and V2G (vehicle-to-grid) modes in order to respond to the load changes in the system can play an important role. Nevertheless, due to having a large number of EVs in the near future, the use of EV Aggregator (EVA) is necessary [1]. Therefore, the contribution of the EVA in power system along with the conventional controller used for frequency control will be a vital task, and it has been one of the main subjects in recent publications for power systems [2]. This participation has mostly been applied on either primary [2] or secondary [3] levels. In the primary level controller decreases the frequency

deviation following any power imbalance, and the secondary level brings the frequency to the nominal value.

For the primary regulation authors in Ref. [4] have suggested a controller in which the half power of the EV is used to regulate the frequency without considering the effect of the time delay originating from the communication links and determining the primary participation gain of the EV optimally. Also, the linear model of the power system, not a real nonlinear system, is used for numerical simulations. In Ref. [5] EVs take part only in the primary frequency control by using the droop method without using an optimal value for the participation gain of EV. The PI controller has only been designed for thermal power plants. Like Ref. [4] the simulations are carried out on a linear model. Authors in Ref. [6] have proposed a fuzzy controller contributing in the primary level of the frequency control by assuming that the participation of EVs is constant. The designed controller is also based on the linear model and it ignores the effect of nonlinearities. Moreover, the linear model of the power system has been used for numerical simulations. Ref. [7] has studied the effect of EVs participating in the frequency regulation on the Bornholm power system. It shows that the frequency stability is improved at the presence of EVs. Also, it has explored the EVs contribution on a single-area power system with the complex dynamic, nonlinearity and voltage dependency. The work has not been extended to a real multi-machine power system.

Some other studies have used EVs in the secondary level of the frequency control. Ref. [8] has suggested a fuzzy controller for EVs participating in the secondary level. The controller settings must be changed according to the different contributions of EVs which makes the controller be hardly useable in a real power system. Ref. [9] designs a common Proportional Integral (PI) controller for both thermal units and EVs based on the linear model of the multi-area power system. Although the results reveal that any change in the contribution of EVs may lead to instability, no discussion and solution have been given. Ref. [10] has suggested the LQR-PID based controller for both thermal plants and EVs. The controller robustness is achieved by using the Linear Matrix Inequality (LMI) approach without considering the time delay originating from the communication links. All simulations are carried out on the linear model of a two-area power system, not a real nonlinear system. Ref. [11] has proposed the H∞ controller by using the state feedback theory with considering the time delay. The proposed structure sends the same signal for both thermal plant and EVA. The method is applied only on a single-area power system and it is not extended to a multi-area power system. Ref. [12] has proposed a common controller for both thermal units and EVs by considering the effect of the time delay. The results show that there is a maximum margin for the time delay. Simulations are carried out on the linear model of the power system without considering Generation Rate Constraint (GRC) effect in the frequency regulation. Ref. [13] has designed a common PD-PI controller for both EVs and power plant by using a modified moth swarm algorithm based on the hybrid fuzzy method without determining the optimal contribution gains of EVs. Ref. [14] gives an adaptive differential evolution based PDF plus (1+PI) controller. The results show that at the presence of EVs the frequency stability can be improved. However, this method experiences the same drawback of Ref. [13]. Ref. [15] has studied the effect of the time delay on the stability of the frequency regulation for a single-area power system. It is shown that the designed controller must consider the time delay as well as the contribution gains of EVs. Nevertheless, the effect of different participation gains of EVs has not been discussed and the study has not been extended to the multi-area power system. Ref. [16] has used Sine Cosine Algorithm (SCA) for designing a Fractional-Order PID (FOPID) controller for EVAs contributing in the frequency regulation. Although this paper considers time delay for tuning the FOPID controller, it ignores the effect of GRC in simulations to ensure that the system performance is satisfactory. Ref. [17] has studied the effect of the time delay on a single-area power system without determining the optimal participation gains of EVs. It is shown that the time delay leads to the instability when the controller is not regulated well.

As mentioned above the participation of EVs in the frequency regulation is highly dependent on the time delay in communication between EVA and EVs, and their contribution in the frequency regulation. This will influence on the system performance if these uncertainties and nonlinearity are not taken into account to design the frequency controller. The capability of the controller can be more doubtful if some other nonlinearities such as Generation Rate Constraint (GRC) are not considered in the design procedure and simulations. Thus, designing a robust controller for EVs is an essential task which has not been the case study in previous works for both levels of the frequency control. In doing so, this paper proposes a robust state feedback controller by considering the time delay

imposed by the communications links for both primary and secondary frequency controls. The problem is first formulated as some LMIs by using the Lyapunov-Krasovskii functional method. Then, the participation gains (both the primary ($K_{P,EV}$) and the secondary ($K_{S,EV}$)) are optimized by Teaching Learning Based Optimization (TLBO) algorithm when the effect of GRC used for the thermal turbine, as a nonlinear element, is taken into account. The simulations are carried out in Power Factory DIGSILENT environment for two different power systems based on the nonlinear models. The results show that the proposed method can provide a better frequency regulation than other methods at the presence of the time delay and uncertainties.

The main contributions of the paper can be summarized as follows;

1. Designing a robust frequency controller based on the state feedback theory for Electric Vehicle aggregators considering the effect of the time delay.
2. Determining the optimal values for the participation gains (for both primary and secondary levels) of EVs to have a desirable performance for any disturbance in power system.
3. EVAs take part in both primary and secondary frequency control.

Also, the effect of GRC is considered in the design procedure and simulations to show that the designed controller is able to a give a stable functioning for different uncertainties and nonlinearity existed in power system.

2. POWER SYSTEM MODEL

Fig. 1 shows the model of area i including EVA from a multi-area power system. For the sake of the simplicity, the subscript i representing the number of the area is hereafter neglected.

For the power plant an integral controller with gain K_I is used for the secondary control and its input is Area Control Error (*ACE*) which is given as

$$ACE = \beta \Delta f + \Delta P_{tie-line} \tag{1}$$

where β is the bias factor. Δf and $\Delta P_{tie-line}$ are the deviations in frequency and tie-line power, respectively. The output of this controller experiences the time delay τ_1 imposed by the communication links. EVA has been presented as a first-order transfer function with time constant T_{EV} [9] participating in both primary and the secondary frequency regulations with $K_{P,EV}$ and $K_{S,EV}$ gains, respectively. Since EVA sends the control signals to every EV individually, this signal encounters a time delay shown by τ_2. In Fig. 1, Δu represents the output signal of the secondary controller for EVA. The inputs of this controller are the states of the system. It is assumed that these states are available by the estimators and observers. The connection of area i to the neighbor area j is modeled by the tie-line synchronous coefficient T_{ij}. Two external disturbances ΔP_L and w are the power change of the load and the effect of the neighbor areas, respectively.

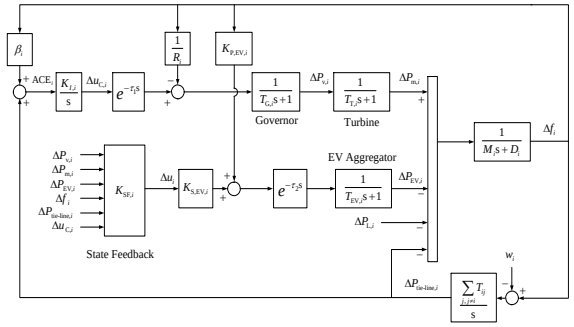

Fig. 1. Linear model of area i from a multi-area power system

2.1. State Space Model of Power System

The first step of designing a state feedback controller is to extract the state space model of the system. The state vector is considered as

$$\Delta \mathbf{x} = \begin{bmatrix} \Delta P_v & \Delta P_m & \Delta P_{\mathrm{EV}} & \Delta f & \Delta u_{\mathrm{C}} & \Delta P_{\text{tie-line}} \end{bmatrix}^T \tag{2}$$

where ΔP_v , ΔP_m , ΔP_{EV} , and $\Delta P_{tie-line}$ are the output power deviations of the governor, turbine, EV, and tie-line power respectively. Δu_C shown in Fig.1 is the output of the integral controller. Consequently, the state space model of the system is obtained as

$$\begin{aligned} \Delta \dot{\mathbf{x}}_i(t) &= \mathbf{A}_i \Delta \mathbf{x}_i(t) + \mathbf{A}_{1,i} \Delta \mathbf{x}_i(t-\tau_1) + \mathbf{A}_{2,i} \Delta \mathbf{x}_i(t-\tau_2) \\ &\quad + \mathbf{B}_i \Delta u_i(t) + \mathbf{E}_i \omega_i(t) \\ z_i(t) &= \mathrm{ACE}_i = \mathbf{C}_{Z,i} \Delta \mathbf{x}_i(t) \end{aligned} \tag{3}$$

where

$$\omega_i(t) = \begin{bmatrix} \Delta P_{\mathrm{L},i} \\ w_i \end{bmatrix} \tag{4}$$

$$\mathbf{A}_i = \begin{bmatrix} -\frac{1}{T_{G,i}} & 0 & 0 & -\frac{1}{T_{G,i} R_i} & 0 & 0 \\ \frac{1}{T_{T,i}} & -\frac{1}{T_{T,i}} & 0 & 0 & 0 & 0 \\ 0 & 0 & -\frac{1}{T_{EV,i}} & 0 & 0 & 0 \\ 0 & \frac{1}{M_i} & -\frac{1}{M_i} & -\frac{D}{M_i} & -\frac{1}{M_i} & 0 \\ 0 & 0 & 0 & \sum_{j,j\neq i} T_{i,j} & 0 & 0 \\ 0 & 0 & 0 & K_{I,i}\beta_i & K_{I,i} & 0 \end{bmatrix} \tag{5}$$

$$\mathbf{A}_{1,i}=\begin{bmatrix}0&0&0&0&0&-\dfrac{1}{T_{G,i}}\\0&0&0&0&0&0\\0&0&0&0&0&0\\0&0&0&0&0&0\\0&0&0&0&0&0\\0&0&0&0&0&0\end{bmatrix} \tag{6}$$

$$\mathbf{A}_{2,i}=\begin{bmatrix}0&0&0&0&0&0\\0&0&0&0&0&0\\0&0&0&\dfrac{K_{\mathrm{P,EV},i}}{T_{EV,i}}&0&0\\0&0&0&0&0&0\\0&0&0&0&0&0\\0&0&0&0&0&0\end{bmatrix} \tag{7}$$

$$\mathbf{B}_i=\begin{bmatrix}0&0&\dfrac{K_{S,EV,i}}{T_{EV,i}}&0&0&0\end{bmatrix}^T \tag{8}$$

$$\mathbf{E}_i=\begin{bmatrix}0&0&0&-\dfrac{1}{M_i}&0&0\\0&0&0&0&-\dfrac{\sum_{j,j\neq i}T_{ij}}{\mathrm{s}}&0\end{bmatrix}^T \tag{9}$$

$$\mathbf{C}_{Z,i}=\begin{bmatrix}0&0&0&1&1&0\end{bmatrix} \tag{10}$$

The controller to be designed in the next section will reduce the effect of the disturbances $\omega_i(t)$ on the output variable $z(t)$ given in Eq. (3).

3. STATE FEEDBACK DESIGN PROCEDURE

The design procedure is carried out in two steps. First, the robust state feedback is formulated by using Lyapunov-Krasovskii functional theory [18]. Then, $K_{P,EV}$ and $K_{S,EV}$ regulation gains are optimally obtained by employing TLBO algorithm.

3.1. State Feedback Design

In this section, the robust state feedback controller is formulated by considering two objectives of the performance and stability. The mathematical representation is carried out as some LMIs. For the simplicity, the subscript *i* representing the number of the area is neglected. The controller design contains three stages: extracting the state space model which is given in Section 2, the robust performance, and the robust stability.

The state feedback can be represented as

$$\Delta u=\mathbf{K}_{\mathrm{SF}}\Delta\mathbf{x}(t-\tau_2) \tag{11}$$

where Δu is the output of the secondary controller for EVAs and K_{SF} is the state feedback vector. Then, the state space model (given in Eq. (3)) considering the state feedback can be written as

$$\begin{aligned}\Delta\dot{\mathbf{x}}&=\mathbf{A}\Delta\mathbf{x}(t)+\mathbf{A}_1\Delta\mathbf{x}(t-\tau_1)+\mathbf{A}_2\Delta\mathbf{x}(t-\tau_2)\\&\quad+\mathbf{B}\mathbf{K}_{\mathrm{SF}}\Delta\mathbf{x}(t-\tau_2)+\mathbf{E}\mathbf{W}\\z&=\mathrm{ACE}=\mathbf{C}_z\Delta\mathbf{x}\end{aligned} \tag{12}$$

Then, the robust performance is achieved by minimizing the effect of the disturbances ($\omega(t)$) on the measured signal (*ACE*). The robust performance can be written as [19]

$$\frac{\|z(t)\|_2}{\|\omega(t)\|_2}\le\gamma^2 \tag{13}$$

where $\|\ \|_2$ is the norm 2 of signal. γ is the attenuation level. The lower attenuation level decreases the effect of the disturbance on the measured signal. Equation (13) can be rewritten as

$$z(t)^T z(t)-\gamma^2\omega(t)^T\omega(t)\le 0 \tag{14}$$

The above inequality will be used with the stability LMIs.

Finally, to achieve the robust stability at the presence of disturbances as well as the parameters variation the Lyapunov-Krasovskii functional is defined as [20]

$$\begin{aligned}V(t)&=\Delta\mathbf{x}^T(t)\mathbf{P}\Delta\mathbf{x}(t)+\int_{t-h_1}^{t}\Delta\mathbf{x}^T(s)\mathbf{Q}_1\Delta\mathbf{x}(s)\mathrm{d}s\\&\quad+\int_{t-h_2}^{t}\Delta\mathbf{x}^T(s)\mathbf{Q}_2\Delta\mathbf{x}(s)\mathrm{d}s\\&\quad+h_1\int_{t-h_1}^{t}\int_{s}^{t}\Delta\dot{\mathbf{x}}^T(\theta)\mathbf{R}_1\Delta\dot{\mathbf{x}}(\theta)\mathrm{d}\theta\mathrm{d}s\\&\quad+h_2\int_{t-h_2}^{t}\int_{s}^{t}\Delta\dot{\mathbf{x}}^T(\theta)\mathbf{R}_2\Delta\dot{\mathbf{x}}(\theta)\mathrm{d}\theta\mathrm{d}s\end{aligned} \tag{15}$$

where P, Q_1, Q_2, R_1 and R_2 are positive definite matrices. h_1 and h_2 are the upper bounds of the τ_1 and τ_2, respectively. If P, Q_1, Q_2, R_1 and R_2 are selected positive definite matrixes, $V(t)$ will be greater than or equal to zero. When $V(t)$ is positive and $\dot{V}(t)$ becomes negative, as shown in Eq. (16) ,the robust stability is achieved [20].

$$\begin{aligned}\dot{V}(t)&=\Delta\dot{\mathbf{x}}^T(t)\mathbf{P}\Delta\mathbf{x}(t)+\Delta\mathbf{x}^T(t)\mathbf{P}\Delta\dot{\mathbf{x}}(t)\\&+\Delta\mathbf{x}^T(t)\mathbf{Q}_1\Delta\mathbf{x}(t)-\Delta\mathbf{x}^T(t-h_1)\mathbf{Q}_1\Delta\mathbf{x}(t-h_1)\\&+\Delta\mathbf{x}^T(t)\mathbf{Q}_2\Delta\mathbf{x}(t)-\Delta\mathbf{x}^T(t-h_2)\mathbf{Q}_2\Delta\mathbf{x}(t-h_2)\\&+h_1\left\{-\int_{t-h_1}^{t}\Delta\dot{\mathbf{x}}^T(\theta)\mathbf{R}_1\Delta\dot{\mathbf{x}}(\theta)\mathrm{d}\theta+h_1\Delta\dot{\mathbf{x}}^T(t)\mathbf{R}_1\Delta\dot{\mathbf{x}}(t)\right\}\\&+h_2\left\{-\int_{t-h_2}^{t}\Delta\dot{\mathbf{x}}^T(\theta)\mathbf{R}_2\Delta\dot{\mathbf{x}}(\theta)\mathrm{d}\theta+h_2\Delta\dot{\mathbf{x}}^T(t)\mathbf{R}_2\Delta\dot{\mathbf{x}}(t)\right\}<0\end{aligned} \tag{16}$$

By using the Jensens' lemma [20], Schur complement [21] and defining $\eta=\begin{bmatrix}\Delta\mathbf{x}(t)^T & \Delta\mathbf{x}^T(t-\tau_1) & \Delta\mathbf{x}^T(t-\tau_2) & \omega(t)^T\end{bmatrix}^T$, $\dot{V}(t)$ can be written as

$$\eta^T \Gamma \eta < 0 \tag{17}$$

where

$$\Gamma = \begin{bmatrix} PA + A^T P + Q_1 + Q_2 - R_1 - R_2 & PA_1 + R_1 & PA_2 + R_2 + PBK_{SF} & PE \\ * & -Q_1 - R_1 & 0 & 0 \\ * & * & -Q_2 - R_2 & 0 \\ * & * & * & 0 \end{bmatrix}$$

$$+h_1^2 \begin{bmatrix} A^T \\ A_1^T \\ A_2^T + K_{SF}^T B^T \\ E^T \end{bmatrix} R_1 \begin{bmatrix} A & A_1 & A_2 + BK_{SF} & E \end{bmatrix} \tag{18}$$

$$+h_2^2 \begin{bmatrix} A^T \\ A_1^T \\ A_2^T + K_{SF}^T B^T \\ E^T \end{bmatrix} R_2 \begin{bmatrix} A & A_1 & A_2 + BK_{SF} & E \end{bmatrix}$$

Consequently, by combining the robust performance (14) and the robust stability (18) criteria, the following LMI is obtained

$$\Psi = \begin{bmatrix} PA + A^T P + Q_1 + Q_2 - R_1 - R_2 & PA_1 + R_1 & PA_2 + R_2 + PBK_{SF} & PE \\ * & -Q_1 - R_1 & 0 & 0 \\ * & * & -Q_2 - R_2 & 0 \\ * & * & * & -\gamma^2 I \end{bmatrix}$$

$$+h_1^2 \begin{bmatrix} A^T \\ A_1^T \\ A_2^T + K_{SF}^T B^T \\ E^T \end{bmatrix} R_1 \begin{bmatrix} A & A_1 & A_2 + BK_{SF} & E \end{bmatrix} \tag{19}$$

$$+h_2^2 \begin{bmatrix} A^T \\ A_1^T \\ A_2^T + K_{SF}^T B^T \\ E^T \end{bmatrix} R_2 \begin{bmatrix} A & A_1 & A_2 + BK_{SF} & E \end{bmatrix}$$

$$+\begin{bmatrix} C_Z^T \\ 0 \\ 0 \\ 0 \end{bmatrix} \begin{bmatrix} C_Z & 0 & 0 & 0 \end{bmatrix} \prec 0$$

If Ψ is negative definite matrix, the LMIs given in Eq. (14) and Eq. (18) will be satisfied. The LMI given in Eq. (19) can be rewritten as

$$\Psi \prec 0 \tag{20}$$

By implementing the congruent transformation, (20) leads to the following LMI.

X is defined as the inverse of P. Then, by multiplying the equation given in Eq. (21) from left and right hand sides with $diag\left(\begin{bmatrix} X & X & X & I & I & I & I \end{bmatrix}\right)$, the following LMI can be calculated by Eq. (22).

$$\begin{bmatrix} PA + A^T P + Q_1 + Q_2 - R_1 - R_2 & PA_1 + R_1 & PA_2 + R_2 + PBK_{SF} \\ * & -Q_1 - R_1 & 0 \\ * & * & -Q_2 - R_2 \\ * & * & * \\ * & * & * \\ * & * & * \\ * & * & * \end{bmatrix}$$

$$\begin{bmatrix} PE & h_1 A^T & h_2 A^T & C_Z^T \\ 0 & h_1 A_1^T & h_2 A_1^T & 0 \\ 0 & h_1 A_2^T + h_1 K_{SF}^T B^T & h_2 A_2^T + h_2 K_{SF}^T B^T & 0 \\ -\gamma^2 I & h_1 E^T & h_2 E^T & 0 \\ * & -R_1^{-1} & 0 & 0 \\ * & * & -R_2^{-1} & 0 \\ * & * & * & -I \end{bmatrix} \prec 0 \tag{21}$$

$$\begin{bmatrix} AX + XA^T + \tilde{Q}_1 + \tilde{Q}_2 - \tilde{R}_1 - \tilde{R}_2 & A_1 X + \tilde{R}_1 & A_2 X + \tilde{R}_2 + BY \\ * & -\tilde{Q}_1 - \tilde{R}_1 & 0 \\ * & * & -\tilde{Q}_2 - \tilde{R}_2 \\ * & * & * \\ * & * & * \\ * & * & * \\ * & * & * \end{bmatrix}$$

$$\begin{bmatrix} E & h_1 XA^T & h_2 XA^T & XC_Z^T \\ 0 & h_1 XA_1^T & h_2 XA_1^T & 0 \\ 0 & h_1 XA_2^T + h_1 Y^T B^T & h_2 XA_2^T + h_2 Y^T B^T & 0 \\ -\gamma^2 I & h_1 E^T & h_2 E^T & 0 \\ * & \tilde{R}_1 - 2X & 0 & 0 \\ * & * & \tilde{R}_2 - 2X & 0 \\ * & * & * & -I \end{bmatrix} \prec 0 \tag{22}$$

where

$$\tilde{Q}_1 = XQ_1X \succ 0$$
$$\tilde{Q}_2 = XQ_2X \succ 0$$
$$\tilde{R}_1 = XR_1X \succ 0$$
$$\tilde{R}_2 = XR_2X \succ 0$$
$$Y = K_{SF}X$$

Finally, Eq. (22) based on the state space model of the system given in Eq. (3) will be solved by using YALMIP Toolbox of MATLAB and matrices $X \succ 0$, $\tilde{Q}_1 \succ 0$, $\tilde{Q}_2 \succ 0$, $\tilde{R}_1 \succ 0$, $\tilde{R}_2 \succ 0$, and Y are obtained. Accordingly, $P \succ 0$, $Q_1 \succ 0$, $Q_2 \succ 0$, $R_1 \succ 0$, and $R_2 \succ 0$ can be derived. Therefore, $V(t)$ in Eq. (15) and $\dot{V}(t)$ in Eq. (16) will be positive and negative, respectively which means that the robust performance and stability are simultaneously satisfied [19]. Then, the state feedback vector can be calculated as

$$Y = K_{SF}X \Rightarrow K_{SF} = YX^{-1} \tag{23}$$

3.2. Teaching Learning Based Optimization

The heuristic optimization algorithms are implemented to solve the engineering problems. These algorithms are

comparatively simple, no need to the gradient of the objective function, and have enough accuracy [22, 23]. In many heuristic algorithms such as PSO, ABC, GA and others a number of different parameters have to be determined and their performances are highly dependent on these settings. In order to solve this drawback, as shown in Refs. [22-24], TLBO, as a population based algorithm, will be used here to find the optimal solutions of the primary ($K_{P,EV}$) and secondary ($K_{S,EV}$) contribution settings of EVs. In this algorithm, there is only the need to allocate the iteration and population size settings. The calculations are divided into learner and teacher phases. The solution candidates are called students. Teacher is a solution which is the best one among all solutions to provide the minimum amount for the objective function in the iterations. For any iteration, the learners' solution is modified in order to move towards the best solution (i.e. teacher solution).

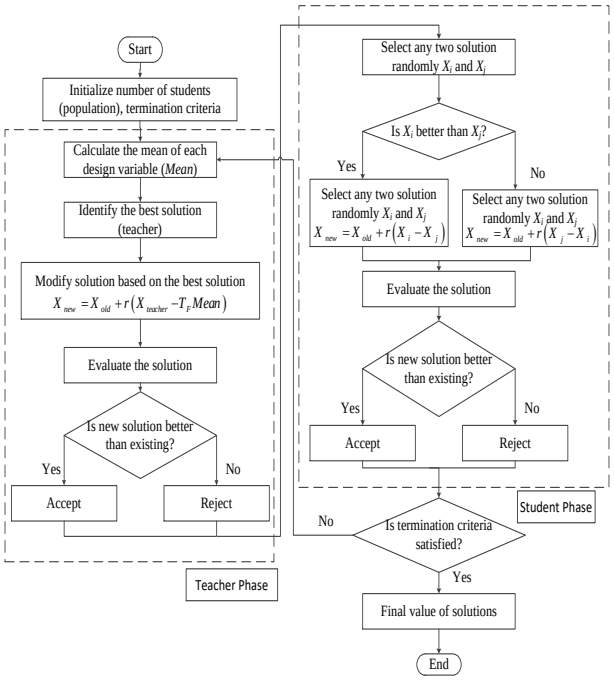

Fig. 2. Flowchart of TLBO algorithm

The optimization flowchart is given in Fig. 2 in which the following steps are to be done.

Step 1: In teacher phase, the mean value for each variable is calculated,

Step 2: The best solution is selected as the teacher (X_{teacher})

Step 3: Each solution according to the following calculation is modified

$$X_{new}=X_{old}+r\left(X_{\text{teacher}}-T_F Mean\right) \tag{24}$$

where T_F is 1 or 2 and r is a random value between 0 and 1.

Step 4: If the new solution obtained by (24) is better than the old solution, the new solution will be accepted. Otherwise, it will be rejected.

Step 5: Two different solutions i and j are selected. If solution i is better than solution j, the solution of i will be modified as

$$X_{new}=X_{old}+r\left(X_i-X_j\right) \tag{25}$$

Otherwise,

$$X_{new}=X_{old}+r\left(X_j-X_i\right) \tag{26}$$

Step 6: If the new solution calculated in Step 5 is better, it will be accepted. Otherwise, it will be rejected.

Step 7: If the termination criterion is satisfied, the algorithm is ended. Otherwise, go back to Step 1.

It should be mentioned that steps 1 to 4 are done in teacher phase and steps 5 to 7 belong to student phase.

The objective function for a power system including n areas is formulated as

$$\min_{K_{P,EV,i},K_{S,EV,i}} \sum_{i=1}^{n}\int\left|ACE_i(t)\right|\mathrm{d}t$$
$$\text{subject to:} \tag{27}$$
$$K_{P,EV}^{\min}\le K_{P,EV,i}\le K_{P,EV}^{\max}$$
$$0\le K_{S,EV,i}\le 1$$

where i is the area number. It should be mentioned that this objective function is optimized by using the real nonlinear power system including GRC.

4. SIMULATION RESULTS

In this section, simulations are carried out on two cases: two-area and three-area power systems. These systems are modeled in DIgSILENT Power Factory software so as to show the effectiveness of the designed controller. The GRC in turbine model is also considered as shown in Fig. 3 [25].

4.1. Case 1: Two-Area Power System

Fig. 4 shows the two-area power system including 4 generators, two loads, two EVAs. The data of this power system can be found in Ref. [26]. G1 and G3 contribute in both primary and secondary frequency regulations. However, G2 and G4 only regulate the frequency in the primary level. The base power is considered 900 MVA.

The optimal integral gains for areas one and two are calculated by TLBO as $K_{I,1}=$-0.1489 and $K_{I,2}=$-0.2821, respectively. The state feedback control is obtained by solving the problem given in Eq. (22) as

$$K_{SF,1}=[-1.1590\times10^{-3}\quad 1.0714\times10^{-5}\quad -4.7644\times10^{-2}\quad 4.9719\quad -2.1486\times10^{-3}\quad 2.1876\times10^{-4}]^T$$

$$K_{SF,2}=[-2.2144\times10^{-3}\quad 1.4298\times10^{-5}\quad -4.7788\times10^{-2}\quad 4.9445\quad -1.8603\times10^{-3}\quad 7.4007\times10^{-4}]^T$$

The optimization problem given in Eq. (24) is also solved to specify $K_{P,EV}$ and $K_{S,EV}$. The secondary gain ($K_{S,EV}$) is obtained 1 for two areas. This means that the highest participation of EV is preferred for the secondary control. The primary participation gains are calculated as 9.5495 and 30.8915 for areas one and two, respectively. As shown in Fig. 5 the convergence of the nonlinear objective function given in Eq. (27) is reached only after 30 iterations.

4.1.1. Scenario 1: Load increase in Area 1 with considering GRC

In this scenario, GRC is considered for turbines. The load in area 1 increases 20 MW (0.0222 pu) at 10s. The frequency variations are shown in Fig. 6. As can be seen from this figure, the frequency variations by the proposed controller is desirable in terms of the speed, lower overshoot and lower undershoot in comparison with the case when EVAs are not used. Also, the proposed method slightly gives a better performance than the method presented in in Ref. [9].

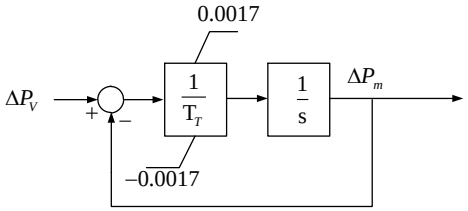

Fig. 3. Turbine model considering the GRC effect

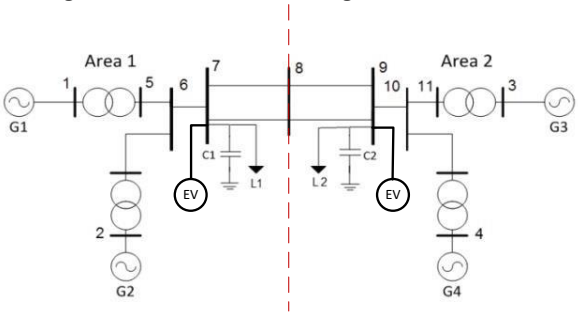

Fig. 4. Two-area power system

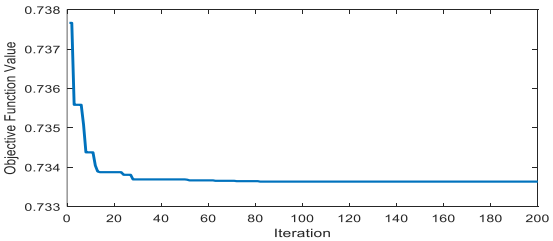

Fig. 5. The convergence curve for two problems of optimizing $K_{P,EV}$ and $K_{S,EV}$

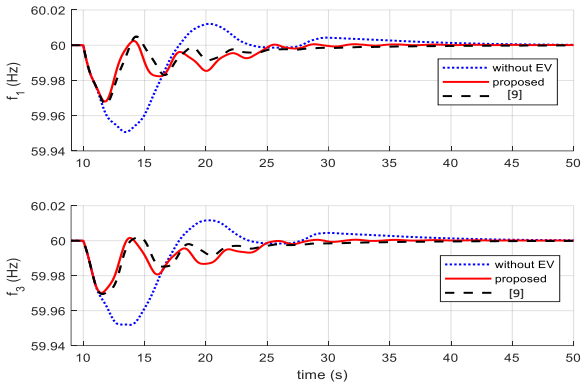

Fig. 6. Frequency variations in areas with the proposed method (solid red), method of Ref. [9] (dashed black), and without EVAs (dotted blue) and optimal setting in case 1, scenario 1

Now, the effect of the optimization for determining the values of the primary ($K_{P,EV}$) and secondary ($K_{S,EV}$) gains are studied. Fig. 7 compares the frequency variations with the optimal and non-optimal values. This figure clearly shows that the system response with the optimal gains is better than two other cases. This shows the importance of the optimization which is not given in the previous works.

4.1.2. Scenario 2: Load increase in area 2 with considering GRC

In this scenario, the load in area 2 increases 30MW (0.0333pu) at 10 s. Fig. 8 shows the proposed controller with the optimal participation gains of EVs. As can be seen from this figure the frequency response is with less oscillation and faster than the case when EVA is not used. Also, the proposed method has less overshoot than that of Ref. [9].

Also, for scenario 2, the frequency response is plotted for different values of $K_{P,EV}$ and $K_{S,EV}$ in Fig. 9. It can be seen that the proposed method with the optimal setting regulates the frequency desirably in comparison with the non-optimal values.

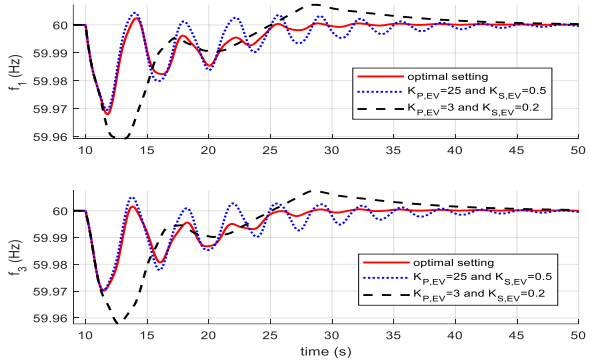

Fig. 7. Frequency variations of proposed method in areas with the optimal setting (solid red), $K_{P,EV}$=3 and $K_{S,EV}$=0.2 (dashed black), and $K_{P,EV}$=25 and $K_{S,EV}$=0.5 (dotted blue) in case 1, scenario 1

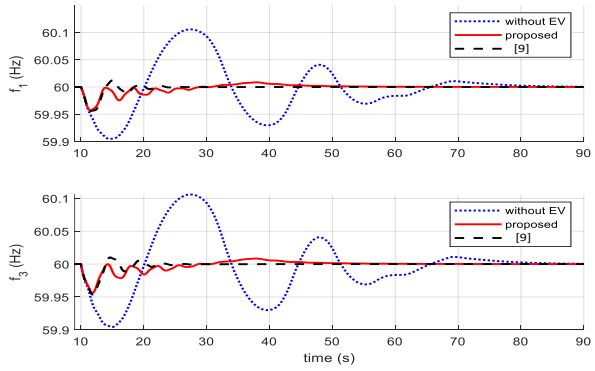

Fig. 8. Frequency variations in areas with the proposed method (solid red), method of Ref. [6] (dash-dotted green), method of Ref. [9] (dashed black), and without EVAs (dotted blue) and optimal setting in case 1, scenario 2

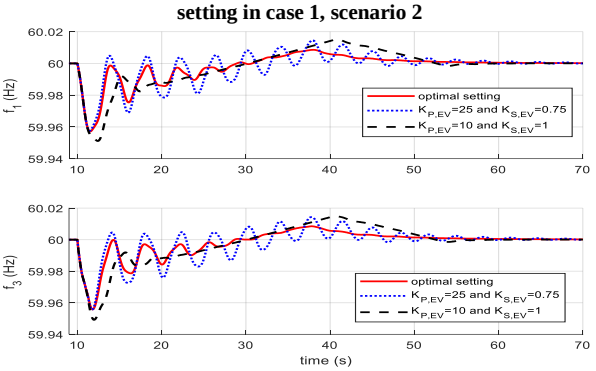

Fig. 9. Frequency variations in areas with the optimal setting (solid red), $K_{P,EV}$=10 and $K_{S,EV}$=1 (dashed black), and $K_{P,EV}$=25 and $K_{S,EV}$=0.75 (dotted blue) in case 1, scenario 2

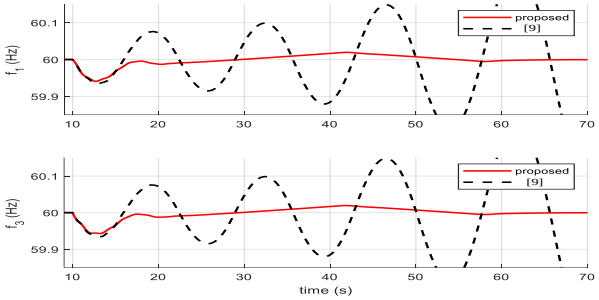

Fig. 10. Frequency variations in areas with the proposed method (solid red), and method of Ref. [9] (dashed black) with $K_{P,EV}$=3 in case 1, scenario 2

As mentioned in Section 1 Ref. [9] shows that for any change in the value of the contributions of EVs the system might be unstable. This will now be tested when $K_{P,EV}$ is changed to 3. As shown in Fig. 10, the frequency response for the method of Ref. [9] is unstable, while for the proposed method the system response is stable and frequency goes back to the nominal value.

4.2. Case 2: IEEE 39-bus Power System

Now the proposed state feedback controller is designed for the IEEE 39-bus power system. Fig. 11 shows the power system including three areas [6]. The data of this system can be found in Ref. [27]. Areas one, two, and three have 3, 2, and 2 generators, respectively. It is supposed that there is 10,000 EVs in each area. With assuming the average demand of each EV as 8 kW, the total demand of EVAs in each area becomes 80 MW. In each area, one generator is responsible for regulating the frequency as the secondary controller; generators 10, 1, and 4 for areas one, two, and three respectively. Also, the controller gains are optimized by using TLBO algorithm through the nonlinear simulation of the power system in DIgSIELNT Power Factory software. The optimized integral gains are calculated as $K_{I,1}$ = -0.1632 , $K_{I,2}$ = -0.0988 and $K_{I,3}$ = -0.2233 for areas one, two, and three, respectively. In simulation results following the load change, the frequency variations of buses 5, 18, and 21 will be shown for areas one, two, and three, respectively.

After solving the problem given in (22), the state feedback controller vectors are obtained as

$$K_{SF,1} = [1.1351\times10^{-2} \quad -2.0034\times10^{-4} \quad -4.6022\times10^{-2} \quad 10.735 \quad 4.7792\times10^{-1} \quad -2.6063\times10^{-3}]^T$$

$$K_{SF,2} = [-1.0600\times10^{-1} \quad 2.3795\times10^{-3} \quad -3.8697\times10^{-2} \quad 7.7251 \quad -1.5112\times10^{-2} \quad -1.8398\times10^{-2}]^T$$

$$K_{SF,3} = [-8.0036\times10^{-2} \quad 8.2893\times10^{-4} \quad -4.1366\times10^{-2} \quad 8.1507 \quad -8.6558\times10^{-3} \quad 1.2500\times10^{-3}]^T$$

for areas one, two, and three, respectively. Then, the participation gains are optimized by using the procedure given in Section 3. Similar to two-area power system, the secondary participation gains are obtained as the maximum value (i.e., 1). Also, the primary participation gains are calculated as 10, 8.2754, and 3.5074 for areas one, two, and three, respectively.

The output signal of the proposed controller is shared between the EVAs according to their available power. In all simulations related to this case, the base power (S_{base}) is considered 1000MVA. Since this system has been used by Ref. [6] to design a controller for the participation of EVs in frequency control, the proposed method is also compared with this reference as well as Ref. [9].

4.2.1. Scenario 1: Load increase in area 1 with considering GRC

In this scenario, the load in area 1 (bus 4) increases 25 MW (0.025pu) at 10 s. Fig. 12 depicts the frequency variations in each area. In this figure, the frequency response with the proposed controller is shown together with the methods of references [6] and [9] and the case when EVA is not used. It is seen that the proposed controller gives a better performance than other cases.

The frequency response for Ref. [6] is oscillatory and is different from that paper because the linear model without considering GRC is used in the design procedure. Also, simulations are done on the linear model. However, the simulations using the method given in Ref. [6] are carried out here in the real nonlinear system. This shows that the designed controller may not have a good performance when the actual nonlinear system is used for simulations and even though the system might be unstable.

Fig. 13 also shows the frequency variations with the load increase as 0.025 pu with the optimized and non-optimized participation gains. From this figure it can be seen that the optimized gains provide a better performance.

4.2.2. Scenario 2: Load Increase in Area 2 with considering GRC

Now, the load in area 2 increases 40 MW (0.040pu) at t=10s. Fig. 14 compares the frequency variations at the presence of EVs (the proposed method and the methods of references [6] and [9]) and at the absence of EVs. It is seen that the proposed controller regulates the frequency better than other cases. In order to show the performance of the optimized gains, the frequency variations in response with the load increase as 0.040 pu is shown in Fig. 15. It is seen that the frequency with the optimized values works better than the non-optimized values. This confirms that the optimization of these values should be considered to design the controller.

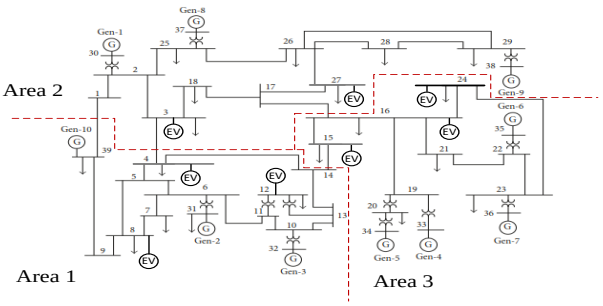

Fig. 11. 39-bus system

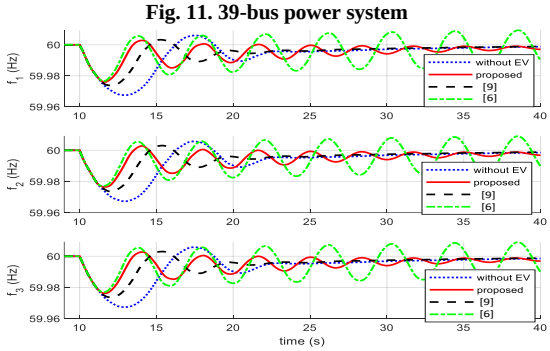

Fig. 12. Frequency variations in areas with the proposed method (solid red), method of Ref. [6] (dash-dotted green), method of Ref. [9] (dashed black), and without EVAs (dotted blue) and optimal setting in case 2, scenario 1

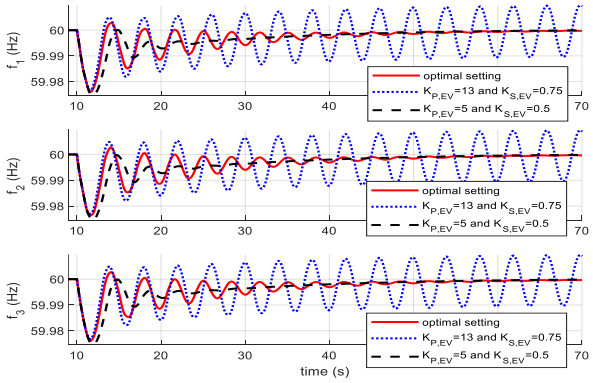

Fig. 13. Frequency variations in areas with the optimal setting (solid red), $K_{P,EV}$=5 and $K_{S,EV}$=0.5 (dashed black), and $K_{P,EV}$=13 and $K_{S,EV}$=0.75 (dotted blue) in case 2, scenario 1

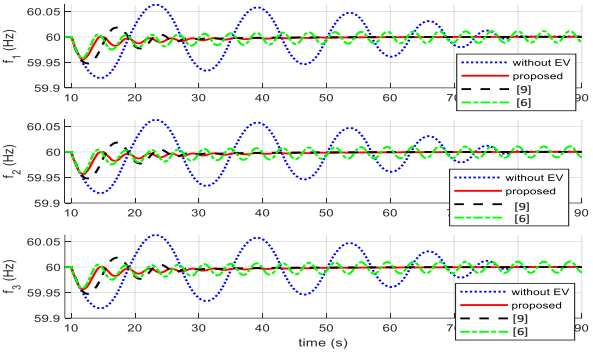

Fig. 14. Frequency variations in areas with the proposed method (solid red), method of Ref. [6] (dash-dotted green), method of Ref. [9] (dashed black), and without EVAs (dotted blue) and optimal setting in case 2, scenario 2

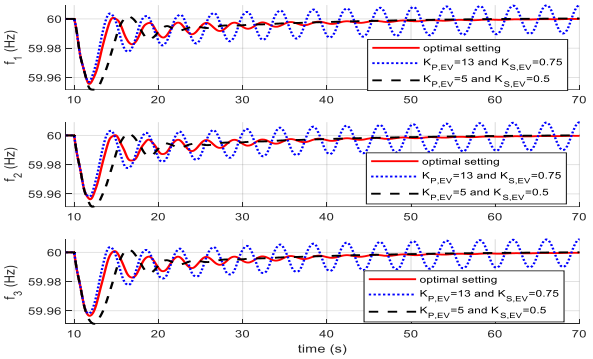

Fig. 15. Frequency variations in areas with the optimal setting (solid red), $K_{P,EV}$=5 and $K_{S,EV}$=0.5 (dashed black), and $K_{P,EV}$=13 and $K_{S,EV}$=0.75 (dotted blue) in case 2, scenario 2

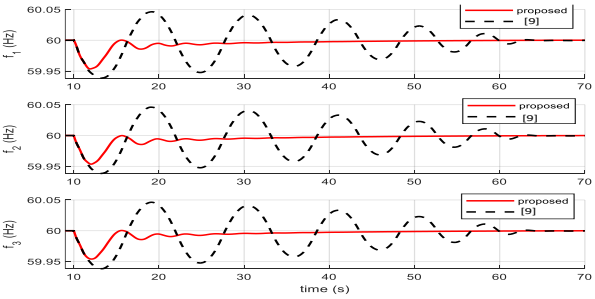

Fig. 16. Frequency variations in areas with the proposed method (solid red), and method of Ref. [9] (dashed black) with $K_{P,EV}$=3 in case 2, scenario 2

Also, to show the robustness feature of the proposed controller, the primary contribution gain ($K_{P,EV}$) is decreased to 3. Following the load change in area 2 (scenario 2), the frequency variations are shown in Fig. 16. It can be seen from this figure that the frequency with the method of Ref. [9] is much more oscillatory than the proposed method. This shows the importance of having a robust controller to overcome the nonlinearities and uncertainties. It should be mentioned that since the method of Ref. [6] presents the simulation results with a constant contribution, its frequency response is not tested for this case.

5. CONCLUSION

This paper proposed a new robust state feedback based controller for EVs aggregators. The design procedure included two steps, the state feedback design and optimizing the primary and the secondary gains of EVAs. First, the state feedback design was obtained by using the Lyapunov-Krasovskii functional method. Different disturbances are considered together with the time delay in the design procedure. In the second step, the primary and secondary gains were optimized by using TLBO. Also, GRC as a nonlinear element in the model of turbine was considered for optimization and simulations. The effectiveness of the proposed controller was shown by executing the simulations on two power systems by using the DIgSILENT Power Factory. The results indicated that the proposed controller regulated the frequency better than other methods for different scenarios. It was shown that the proposed controller worked well in different conditions, especially when the primary and secondary gains of the EVs contributions in frequency regulation are optimized. In order to apply the proposed method in real applications, it is necessary to have the reliable communication links between aggregator and each EV. In the future, the real time communication technologies such as Internet of Things (IoT) and smart grid infrastructure can facilitate this limitation. Further studies on the current topic are recommended in order to study the contribution of EVs in the tertiary level of the frequency control.

REFERENCES

[1] S. Izadkhast et al, “An aggregate model of plug-in electric vehicles including distribution network characteristics for primary frequency control”, *IEEE Trans. Power Syst.*, vol. 31, no. 4, pp. 2987-98, 2016.

[2] S. Izadkhast et al, “Design of plug-in electric vehicle's frequency-droop controller for primary frequency control and performance assessment”, *IEEE Trans. Power Syst.*, 2017.

[3] A. Janjic et al, “Commercial electric vehicle fleet scheduling for secondary frequency control”, *Electr. Power Syst. Res.*, vol. 147, pp. 31-41, 2017.

[4] Y. Ota et al, “Autonomous distributed V2G (vehicle-to-grid) satisfying scheduled charging”, *IEEE Trans. Smart Grid*, vol. 3, no. 1, pp. 559-64, 2012.

[5] S. Vachirasricirikul and I. Ngamroo, “Robust LFC in a smart grid with wind power penetration by coordinated V2G control and frequency controller”, *IEEE Trans. Smart Grid*, vol. 5, no. 1, pp. 371-380, 2014.

[6] S. Falahati Aliabadi, S. Taher, and M. Shahidehpour, “Smart deregulated grid frequency control in presence of renewable energy resources by EVs charging control”, *IEEE Trans. Smart Grid*, vol. 9, no. 2, pp. 1073-85, 2018.

[7] A. Zecchino et al, “Large-scale provision of frequency control via V2G: The Bornholm power system case”, *Electr. Power Syst. Res.*, vol. 170, pp. 25-34, 2019.

[8] S. Falahati, S. Taher, and M. Shahidehpour, “Grid secondary frequency control by optimized fuzzy control of electric vehicles”, *IEEE Trans. Smart Grid*, vol. 9, no. 6, pp. 5613-21, 2018.

[9] K. Ko and D. Sung, “The effect of EV aggregators with time-varying delays on the stability of a load frequency control system”, *IEEE Trans. Power Syst.*, vol. 33, no. 1, pp. 669-680, 2018.

[10] S. Das et al, “High-performance robust controller design of plug-in hybrid electric vehicle for frequency regulation of smart grid using linear matrix inequality approach”, *IEEE Access*, vol. 7, pp. 116911-24, 2019.

[11] D. Aravindh et al, “Design of observer-based non-fragile load frequency control for power systems with electric vehicles”, *ISA Trans.*, vol. 91, pp. 21-31, 2019.

[12] S. Zhou, H. Zeng, and H. Xiao, “Load frequency stability analysis of time-delayed multi-area power systems with EV aggregators based on bessel-legendre inequality and model reconstruction technique”, *IEEE Access*, vol. 8, pp. 99948-55, 2020.

[13] D. Khamari, R. Sahu, and S. Panda, “A modified moth swarm algorithm-based hybrid fuzzy PD–PI controller for frequency regulation of distributed power generation system with electric vehicle”, *J. Control, Autom. Electr. Syst.*, vol. 31, pp. 675-92, 2020.

[14] D. Khamari, R. K. Sahu, and S. Panda, “Adaptive differential evolution based PDF plus (1+ PI) controller for frequency regulation of the distributed power generation system with electric vehicle”, *Int. J. Ambient Energy*, pp. 1-15, 2020.

[15] A. Naveed, Ş. Sönmez, and S. Ayasun, “Impact of electric vehicle aggregator with communication time delay on stability regions and stability delay margins in load frequency control system”, *J. Modern Power Syst. Clean Energy*, vol. 9, no. 3, pp. 595-601, 2021.

[16] F. Babaei and A. Safari, “SCA based fractional-order PID controller considering delayed EV aggregators”, *J. Oper. Autom. Power Eng.*, vol. 8, no. 1, pp. 75-85, 2020.

[17] F. Babaei, A. Safari, and J. Salehi, “Evaluation of delays-based stability of LFC systems in the presence of electric vehicles aggregator”, *J. Oper. Autom. Power Eng.*, vol. 10, no. 2, pp. 165-174, 2022.

[18] C. Ebenbauer and F. Allgower, “Stability analysis for time-delay systems using rekasius's substitution and sum of squares”, *Decision Control, 2006 45th IEEE Conf.*, 2006.

[19] C. Peng and J. Zhang, “Delay-distribution-dependent load frequency control of power systems with

probabilistic interval delays", *IEEE Trans. Power Syst.*, vol. 31, no. 4, pp. 3309-17, 2016.
[20] K. Gu, J. Chen, and V. Kharitonov, "Stability of time-delay systems*", Springer Sci. Business Media*, 2003.
[21] S. Boyd et al, "Linear matrix inequalities in system and control theory", *Philadelphia: Soc. Ind. Appl. Math.*, 1994.
[22] T. Gorripotu et al, "TLBO algorithm optimized fractional-order PID controller for AGC of interconnected power system", *Soft Comput. Data Analytics*, pp. 847-855, 2019.
[23] B. Sahu et al, "A novel hybrid LUS–TLBO optimized fuzzy-PID controller for load frequency control of multi-source power system", *Int. J. Electr. Power Energy Syst.*, vol. 74, pp. 58-69, 2016.
[24] G. Chicco and A. Mazza, "Heuristic optimization of electrical energy systems: Refined metrics to compare the solutions", *Sustain. Energy, Grids Net.*, vol. 17, p. 100197, 2019.
[25] C. Lu, C. Liu, and C. Wu, "Effect of battery energy storage system on load frequency control considering governor deadband and generation rate constraint", *IEEE Trans. Energy Conv.*, vol. 10, no. 3, pp. 555-561, 1995.
[26] P. Kundur, N. Balu, and M. Lauby, "Power system stability and control", New York: McGraw-Hill, 1994.
[27] I. Hiskens, "IEEE PES task force on benchmark systems for stability controls", *Tech. Rep.*, 2013.